nanomaterials

MDPI

Article

2.72 μm Passively Q-Switched Bulk Laser with the Cr_2Te_3 Saturable Absorber Mirror

Hua Wen [1,*], Junhao Cai [1], Maodan Xu [1], Hongying Mei [1], Zhihao Li [2], Shuxiang Sun [1] and Tinglun Xing [2,*]

[1] School of Electronic Information, Huanghuai University, Zhumadian 463000, China
[2] International Joint Research Laboratory of New Energy Materials and Devices of Henan Province, School of Physics and Electronics, Henan University, Kaifeng 475004, China; 15703912205@163.com
* Correspondence: wenhua6@huanghuai.edu.cn (H.W.); tlxing@henu.edu.cn (T.X.)

Abstract

Exploring nanomaterials-based saturable absorber (SA) with high performance plays a crucial role in the development of high-repetition-rate pulsed lasers operating in the mid-infrared band. Herein, we synthesized the Cr_2Te_3 polycrystalline powder by the solid-phase sintering method, and its nanoparticle film was demonstrated to have excellent saturable absorption properties at 2.72 μm, with modulation depths of ~4.5% and an effective nonlinear absorption coefficient of −2.79 cm/MW. When used as an SA in an Er:YAP bulk laser, it enabled Q-switched operation at 2.72 μm. The maximum average output power was 0.61 W at an absorbed pump power of ~6.8 W, with a pulse duration of 266 ns and a repetition rate of 165.6 kHz. These results indicate that Cr_2Te_3 film can be used as efficient optical switch for high-repetition-rate pulsed lasers at 2.7 μm.

Keywords: bulk lasers; 2.72 μm; passive Q-switched; Cr_2Te_3 saturable absorber

1. Introduction

Pulsed lasers with high repetition rates at ~2.7 μm are indispensable in application fields, including gas fingerprinting, medical diagnostics, laser surgery, and so on [1–4]. Er^{3+}-doped bulk lasers emitting around 3 μm have garnered widespread attention due to the superiority of high-compactness and high-efficiency [5,6]; especially, low-doped laser crystals or low-pump-intensity laser systems tend to favor the generation of 2.7 μm laser emission [7,8]. The Q-switching or mode-locking techniques based on passive optical switches provide an effective means to obtain high-repetition-rate pulsed lasers [9,10]. Effective saturable absorption arising from the third-order nonlinearity of nanomaterial thin films has greatly increased the number of available optical switches. Up to now, with the development of nanomaterials and nanophotonic, pulsed lasers based on nanomaterial SAs for passive Q-switching have also made great progress, owing to their cost advantage, effectiveness and high compactness [11,12]. To the best of our knowledge, the nanomaterials, such as graphene [13], phosphorene [14], transition metal dichalcogenides (TMDs) [15,16], topological insulators [17,18], MXenes [19], etc., have been applied to Q-switched laser systems for high-repetition-rate pulsed laser generation. Consider the pulsed bulk lasers operating at ~3 μm; for example, in 2025, Xing et al. reported a short-pulsed passively Q-switched 2.8 μm Er:YAP laser based on VS_2/tellurene composite SA [20]. Zhang et al. achieved an Fe,Cr:ZnS-SA passively Q-switched Er:YAP laser at 2.7 μm [21]. Li et al. reported the nonlinear optical properties of the violet phosphorus SA at ~2.8 μm, as well as its passive Q-switching application in the Er:YAP bulk lasers [22]. Although nanomaterial-based passive modulators in the mid-infrared band have achieved some progress, they are

Check for updates

Academic Editor: Clemens Burda

Received: 28 September 2026
Revised: 13 November 2026
Accepted: 16 November 2026
Published: 18 November 2026

Copyright: © 2026 by the authors. Licensee MDPI, Basel, Switzerland. This article is an open access article distributed under the terms and conditions of the Creative Commons Attribution (CC BY) license.

still relatively scarce compared with their near-infrared counterparts. Consequently, the exploration of more nanomaterials with excellent saturable absorption properties, as well as their applications, remains a valuable research topic.

Chromium(III) telluride (Cr_2Te_3), a member of the TMD family, has attracted growing interest in fields such as magnetic materials science and frictional nanogenerator applications owing to its excellent ferromagnetic and electrical properties [23–25]. However, the research on its optical properties is relatively scarce, although some studies have revealed that Cr_2Te_3 not only has favorable saturable absorption properties in the near-infrared band [26,27], but also exhibits a narrow optical band gap [28,29], which collectively contribute to the potential of nonlinear optical responses and applications in the mid-infrared region. To the best of our knowledge, Cr_2Te_3 has only been used as SA in 1.5 μm fiber laser systems for Q-switching operations [27]. Many of its nonlinear characteristics in the mid-IR bands remain largely unexplored. Therefore, further systematic investigations into its nonlinear optical properties and potential applications in the mid-infrared band are highly warranted. Such research may yield a usable SA material suitable for mid-infrared laser systems.

In this paper, the Cr_2Te_3 polycrystalline powder was synthesized via solid-phase sintering, and its nanoparticle film saturable absorber mirror (SAM) was prepared based on a gold-plated reflector. Open-aperture Z-scan measurements ~2.7 μm revealed its excellent saturable absorption properties, with a modulation depth of ~4.5% and a saturation intensity of 0.18 MW/cm^2. With the transmissive Cr_2Te_3 SA, a ~2.7 μm passively Q-switched Er:YAP bulk laser was achieved. The threshold of the Q-switching laser was ~ 3.4 W, the maximum average output power was 0.61 W when the absorbed pump power was ~6.8 W, with a pulse duration of 266 ns and a repetition rate of 165.6 kHz. These results indicate that Cr_2Te_3 film can be used as efficient optical switch for high-repetition-rate pulsed lasers at 2.72 μm. These results verify that the Cr_2Te_3 film can act as efficient optical switch in the mid-infrared range.

2. Synthesis and Characterization of Cr_2Te_3 Polycrystalline Powder

The Cr_2Te_3 polycrystalline powder was synthesized via solid-phase sintering. The preparation method is as follows: Initially, 208.0 mg of Chromium powder and 765.6 mg of tellurium powder were mixed in a mortar and transferred to a quartz tube. The tube loaded with the raw materials was evacuated to a vacuum of 6×10^{-3} Pa based on a vacuum system and sealed under a hydrogen–oxygen flame. The sealed quartz tube was subsequently subjected to a two-stage sintering process: first held at ~300 °C for 2 h, followed by extended sintering at an optimized temperature of ~1050 °C for more than 30 h. After cooling, the tube was opened and the as-prepared sample, exhibiting a dark green color, was collected.

To characterize the quality of the as-prepared sample, we used Raman spectroscopy, X-ray diffraction (XRD), and energy-dispersive X-ray spectroscopy (EDS) (XFlash 6130, Bruker, Zhengzhou, China) in combination. Raman spectroscopy, as shown in Figure 1a, characterizes the vibrational properties of the Cr_2Te_3 sample. The two characteristic peaks were observed at ~126.2 cm^{-1} and ~144.5 cm^{-1}, which is consistent with previously reported results [30], corresponding to the in-plane Eg mode and the out-of-plane Ag mode. The XRD pattern, as shown in Figure 1b, could characterize the crystal structure of the Cr_2Te_3 sample. The measured diffraction peaks were consistent with the standard Cr_2Te_3 card (PDF#97-004-1940). The energy-dispersive X-ray spectroscopy (EDS) spectrum could characterize the chemical composition ratio of the Cr_2Te_3 sample, as shown in Figure 1c. The measurement results confirmed that the atomic ratio of tellurium to chromium is close to 3:2. The scanning electron microscopy (SEM) illustration in Figure 1c could reveal the elemental distribution of chromium and tellurium.

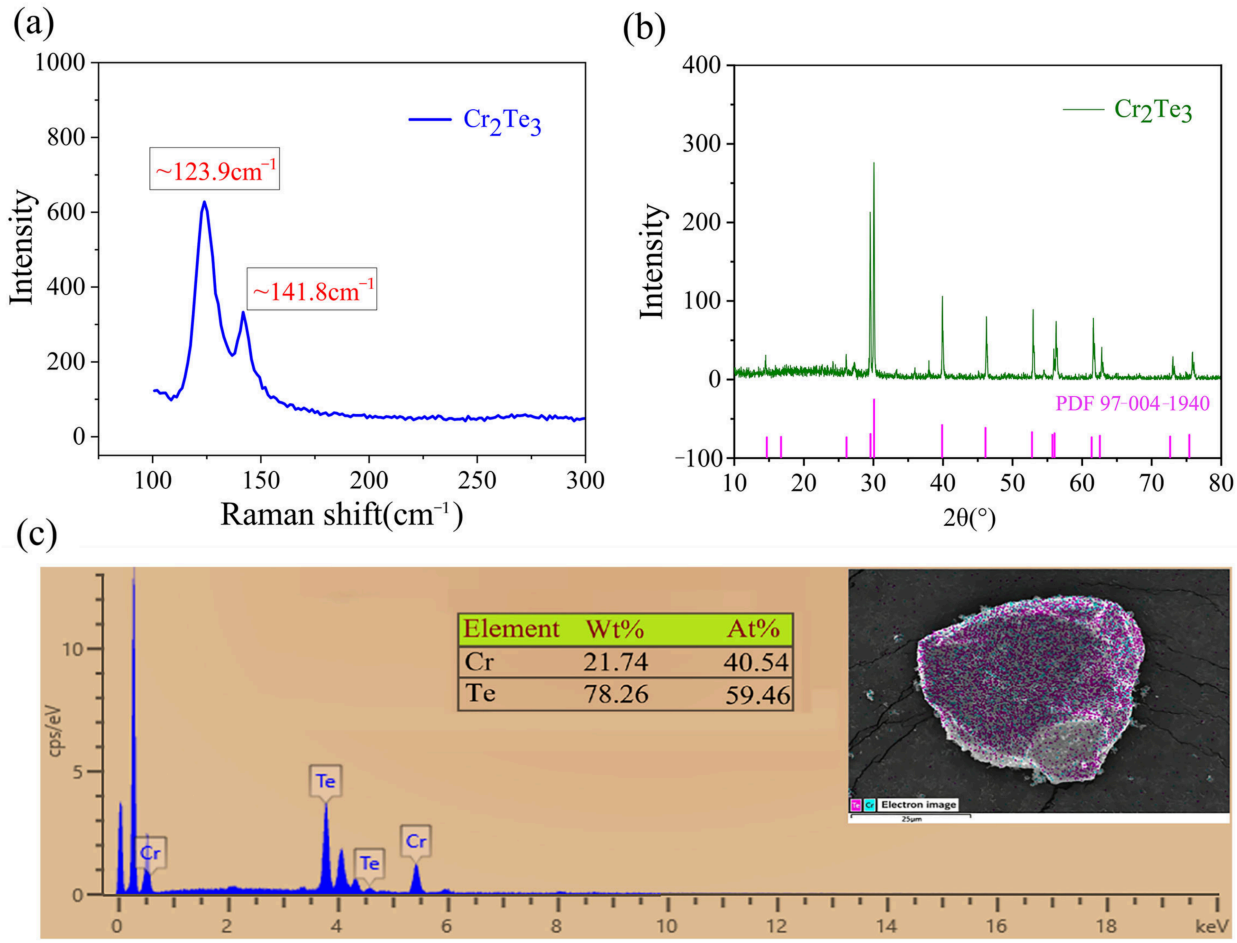


Figure 1. (**a**) The Raman spectra of Cr_2Te_3 sample, (**b**) The X-ray diffraction pattern of Cr_2Te_3 sample, and (**c**) The energy-dispersive X-ray spectroscopy of Cr_2Te_3 sample.

3. Preparation and Characterization of Cr_2Te_3 Saturable Absorber Mirror

Based on the Cr_2Te_3 polycrystalline powder prepared above, a high-quality Cr_2Te_3 film was prepared on a gold-coated silicon mirror through a combined liquid-phase exfoliation (LPE) and spin-coating approach. Specifically, 18 mg of the as-prepared Cr_2Te_3 polycrystalline powder was added to a centrifuge tube containing 6 mL of N-methyl-2-pyrrolidone (NMP), and the mixture was treated with an ultrasonic processor for ~20 h at ~480 W. After centrifugation at 5400 rpm for 10 min, the supernatant was collected and drop-cast onto the same mirror, then spin-coated under optimized conditions. Finally, the sample was vacuum-dried at 60 °C for 6 h, affording a reflective Cr_2Te_3 SAM.

Figure 2a shows the Raman spectra of the Cr_2Te_3 SAM sample. The weak peak at ~125 cm^{-1} is assigned to the A1g mode of the Cr_2Te_3 thin film, consistent with our previous measurements on polycrystalline Cr_2Te_3 powder. The out-of-plane Ag mode at ~144.5 cm^{-1} was not observed, which we attribute to further weakening of this peak at the nanoscale. Figure 2b presents the XRD pattern of the Cr_2Te_3 SAM sample, where a pronounced diffraction peak from the Au thin film appears at ~39°, and a very weak diffraction peak from the Cr_2Te_3 thin film appears at ~31.2°, indexed to the (200) plane.

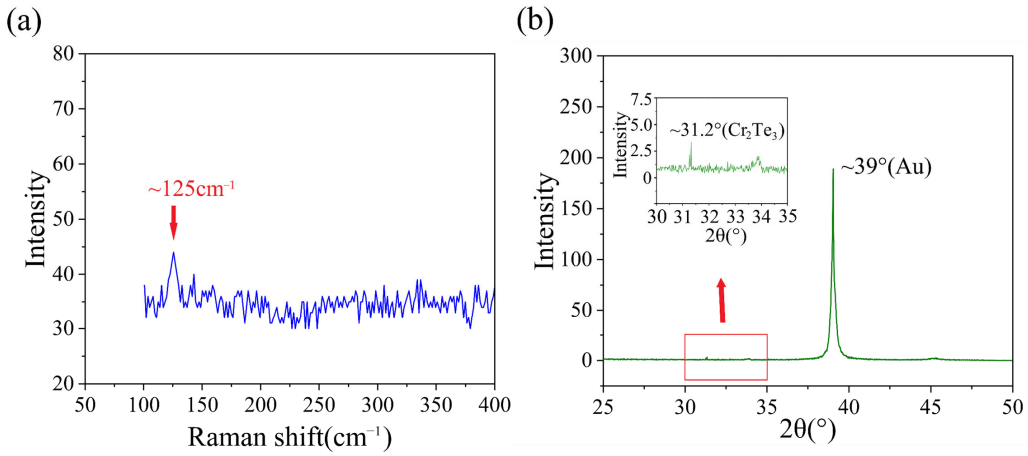


Figure 2. (**a**) The Raman spectra of the Cr_2Te_3 SAM sample and (**b**) the X-ray diffraction pattern of the Cr_2Te_3 SAM sample.

Atomic force microscopy (AFM) was used to characterize the lateral size distributions of the Cr_2Te_3 nanoparticles. The aforementioned supernatant was diluted ~10 times with NMP and coated onto the gold reflector by spin coating to make the nanoparticles distinguishable. Figure 3a displays the 2D image, and Figure 3b presents the corresponding height profiles and lateral dimensions of some nanoparticles, from which we can see that the corresponding lateral dimensions were ~20 nm, and the vertical dimension was in the range of 10-15 nm. Thus, the as-prepared Cr_2Te_3 exhibits a nanoparticle morphology.

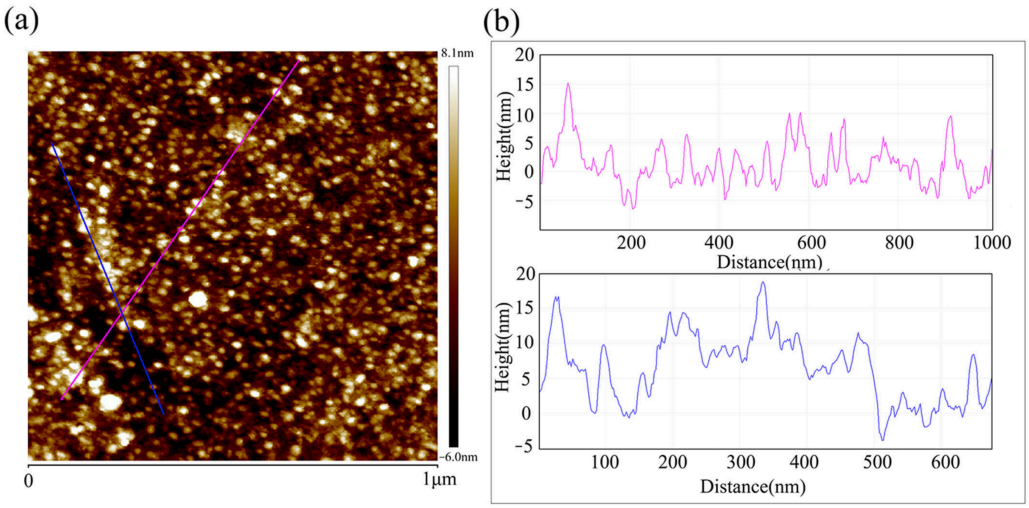


Figure 3. (**a**) The 2D AFM image of Cr_2Te_3 nanoparticles and (**b**) the profiles of Cr_2Te_3 nanoparticles.

An open-aperture Z-scan system at 2.7 μm, based on a pulsed PPMgLN-OPO laser source, was used to investigate the nonlinear optical absorption characteristics of Cr_2Te_3 SAM. The measured results, as shown in Figure 4, indicate that the prepared Cr_2Te_3 SAM exhibits strong saturable absorption at 2.7 μm. The experimental data presented in Figure 4b were fitted using the following expression [15]:

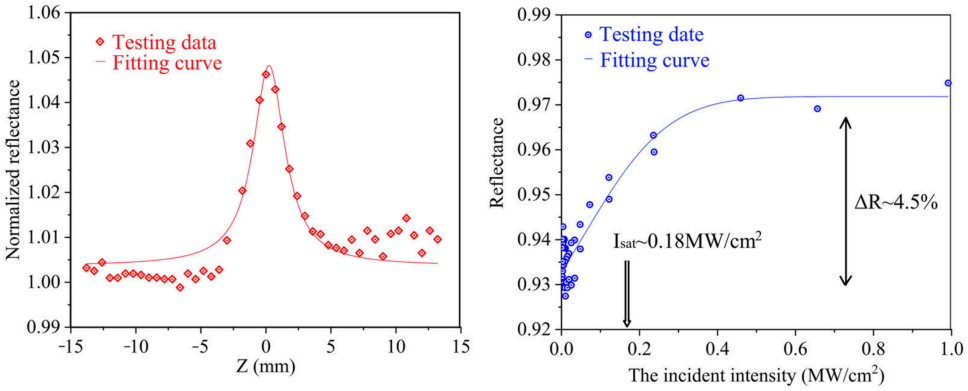
$$R(I) = 1 - \Delta R \cdot \exp\left(\frac{-I}{I_{sat}}\right) - R_{ns} \quad (1)$$

where $R(I)$, ΔR, I, I_{sat} and R_{ns} represent the reflectance, the modulation depth, the incident intensity, the saturable intensity, and the total unsaturated loss, respectively. According to the fitting curve, the modulation depth and saturation intensity were estimated to be

~4.5% and ~0.18 MW/cm^2, respectively. The nonlinear absorption coefficient β_{eff} of the as-prepared Cr_2Te_3 film can be obtained by the following expression [31]:

$$R(z) = \sum_{n=0}^{\infty} \left(-\beta_{eff} I_0 L_{eff}\right)^n / (1 + Z^2/Z_0^2)(n+1)^{3/2} = 1 - \beta_{eff} I_0 L_{eff} / 2^{3/2}(1 + Z^2/z_0^2) \quad (2)$$

where I_0 is the laser intensity at the focus, Z_0 is the Rayleigh length, and L_{eff} is the effective thickness. The effective nonlinear absorption coefficient β_{eff} was estimated to be ~−2.79 cm/MW.



(**a**) (**b**)

Figure 4. (**a**) The Z-scan curve of Cr_2Te_3 SAM at 2.7 μm. (**b**) Nonlinear reflectance versus incident intensity at 2.7 μm.

4. Performance and Discussion of the 2.72 μm Passively Q-Switched Er:YAP Bulk Laser

The Z-scan measurement result of the Cr_2Te_3 SAM reveals strong saturable absorption at 2.7 μm, indicating its great potential for photonic switching applications. To verify its practical utility, we built a passively Q-switched Er:YAP bulk laser experiment with the SAM. Figure 5 presents the schematic of the experimental setup. A 975.5 nm diode laser with a coupled fiber core diameter of 105 μm and a numerical aperture of 0.22 served as the pump source. The pump beam was focused into the center of the Er:YAP crystal with a waist radius of ~0.3 mm by an optical focusing system. A plano–plano resonator ~22 mm long was employed. M_2, designed for high transmission at 975 nm and an optimized transmittance of 2.5% at 2.7 μm, acted as both the input and output coupler. M_1 was either a high-reflectivity mirror or the Cr_2Te_3 SAM. M_3 was a 45° beam splitter exhibiting high transmission at 975 nm and high reflection at 2.7 μm, enabling efficient outcoupling of the mid-infrared laser emission. A filter, designed for high reflection at 975 nm and high transmission at 2.7 μm, was used to block the trace amount of residual pump light from entering the power detector. The gain medium was an Er^{3+}-doped YAP crystal with a doping concentration of 10 at.%, cut to dimensions of 2 × 2 × 10 mm^3. The crystal was held by a copper heat sink maintained at approximately 15 °C.

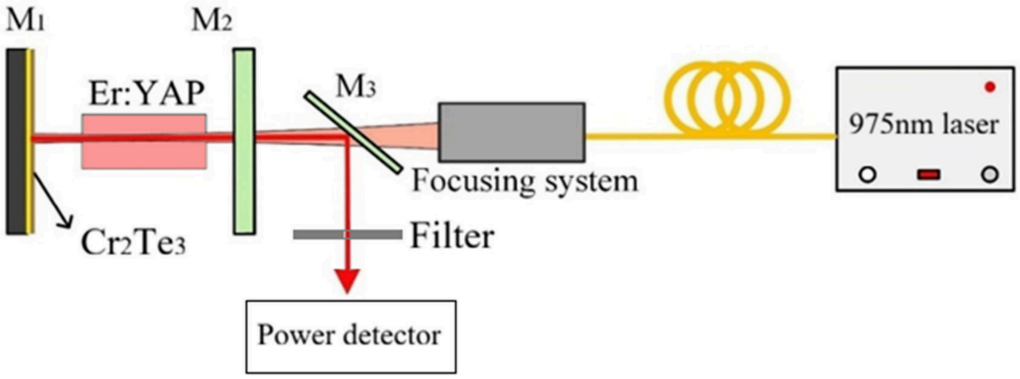


Figure 5. The schematic of the experimental setup.

To compare with the passively Q-switched laser operation and further evaluate the overall optical performance of the above-mentioned Cr_2Te_3 SAM, we initially realized continuous-wave (CW) laser operation by using a high-reflectivity mirror as the cavity mirror (M_1). The measured correlation between the CW output power and the absorbed pump power is illustrated in Figure 6a. The oscillation threshold of the continuous-wave laser was ~1.6 W, demonstrating the low-threshold nature of continuous-wave laser operation. As the pump power increased, the output power of the mid-infrared laser increased almost linearly. When the absorbed pump power reached approximately 6.8 W, the maximum output power was about 1.02 W, corresponding to a slope efficiency of approximately 19.2%. The CW spectrum, measured with a resolution of ~20 nm, is shown in Figure 6b, and the central wavelength was approximately 2.72 μm. As the pump power was further increased, the emission wavelength shifted toward longer wavelengths, as shown in the inset of Figure 6b. Then, the cavity mirror (M_1) was replaced with a reflective Cr_2Te_3 SAM, and stable Q-switched operation was detected once the absorbed pump power surpassed 3.4 W. However, when the pump power was between approximately 2.4 W and 3.4 W, the laser still operated in CW mode, indicating that the Cr_2Te_3 SAM did not trigger saturable absorption at this stage due to the low intracavity laser power density, which is consistent with the trend reported in previously published work [32,33]. The characteristic curve depicting the average output power as a function of the absorbed pump power is also presented in Figure 6a. It shows the same behavior as in the CW mode; the output power of the mid-infrared laser increases almost linearly with increasing pump power. At an absorbed pump power of about 6.8 W, the average output power reached 0.61 W, accompanied by a slope efficiency of approximately 13.5%. Clearly, compared with continuous-wave operation, the output power is significantly lower, primarily because the overall non-saturable loss of the Cr_2Te_3 SAM exceeds that of the dielectric-coated, high-reflectivity cavity mirror. In addition, the central wavelength was measured to be at 2.72 μm, which is consistent with that obtained during CW laser operation.

To investigate the characteristics of the passively Q-switched output laser, the real-time pulse train and temporal waveform were detected using a combination of a fast photodetector (PVM-10.6, VIGO, Poland) with a response time of less than 2 ns and a digital oscilloscope (RIGOL MSO 5354, China). As shown in Figure 7a, the dependence of the repetition rate and pulse width on the absorbed pump power was investigated. As the absorbed pump power increased, the pulse width decreased inversely, from 570 ns at 3.4 W to 266 ns at 6.8 W, while the repetition rate exhibited an approximately linear increase, specifically increasing from 76 kHz to 165.6 kHz. As is typical for most nanomaterials, this behavior is consistent with the fundamental characteristics of passive Q-switching. As the pump power continued to increase, the pulse train exhibited instability and even vanished. We analyze the reason to be that, under higher pump power conditions, a mismatch occurs

between the modulation depth of the saturable absorber mirror and the high gain of the laser crystal. In addition, the single-pulse energy and peak power was calculated, and the detailed variations in single-pulse energy and peak power with absorbed pump power is present in Figure 7b. Clearly, both the single-pulse energy and the peak power increase almost linearly with increasing pump power. The maximum peak power was determined to be 13.9 W, corresponding to a single-pulse energy of 3.7 μJ. Figure 7c displays the pulse trains at absorbed pump powers of 3.4 W, 4 W, and 6.8 W, corresponding to repetition rates of 76 kHz, 104.3 kHz, and 165.6 kHz, respectively. Figure 7d displays the narrowest pulse width of 266 ns with a repetition rate of 165.6 kHz when the absorbed pump power was 6.8 W. These results indicate that the reflective Cr_2Te_3 SAM is a practical optical modulation device at 2.72 μm. Table 1 gives a summarization of some reports on ~2.7 μm passively Q-switched bulk laser based on 2D-material SAs for comparison. By comparison, this work achieves a relatively high average output power, indicating broader application prospects. The Cr_2Te_3 SA film prepared in this study is a nanoparticle thin film with particle sizes predominantly in the 10–15 nm range. Such nanoscale dimensions not only give rise to pronounced size effects but also enhance film uniformity.

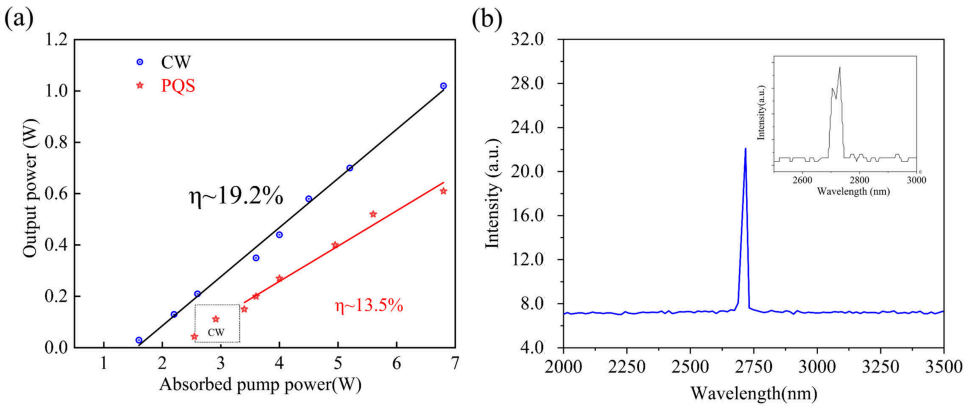


Figure 6. (**a**) Output power of CW and PQS regimes as a function of absorbed pump power. (**b**) PQS output spectrums.

The underlying mechanism is that nanoparticles can act as nucleation sites or fill microdefects during drying, which suppresses local compositional enrichment and thickness fluctuations to form smoother, denser films with better coverage [34]. The reflective Cr_2Te_3 SAM fabricated on a gold-coated mirror substrate exhibits a relatively low total non-saturable loss, which reduces energy loss during laser operation and minimizes slope efficiency degradation.

Table 1. Comparing the performance of the 2.72 μm passively Q-switched Er:YAP bulk laser with different nanomaterial SAs.

SA	*Modulation Depth (%)*	*Average Output Power (mW)*	*Pulse Width (ns)*	*Repetition Frequency (kHz)*	*RF*
$Au/CsPbI_3$	4.17	198	185	375	[35]
$SnSe_2$	11.2	208	198	317	[36]
NiV-LDH	6.7	200	141	295	[19]
Cr_2Te_3	4.5	610	266	165.6	This work

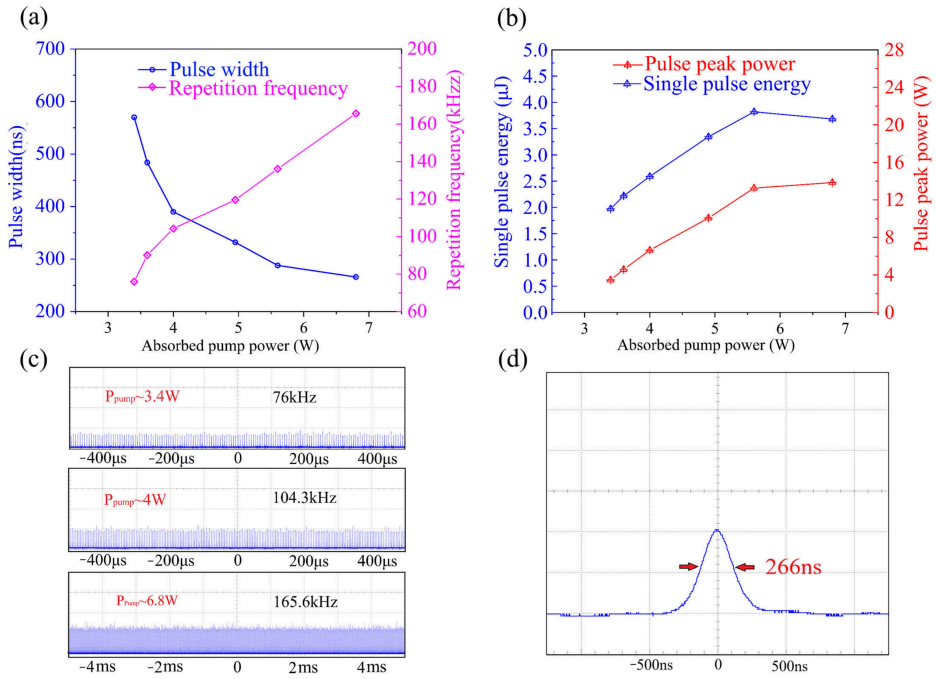


Figure 7. (**a**) Repetition rate and pulse width evolution under different pump absorption. (**b**) Single-pulse energy and pulse peak power evolution under different pump absorption. (**c**) Orderly pulse sequences. (**d**) The narrowest temporal pulse duration.

5. Conclusions

In this study, Cr_2Te_3 powder was synthesized via solid-state reaction in a muffle furnace, and a Cr_2Te_3 SAM with superior saturable absorption properties was prepared and characterized. Open-aperture Z-scan measurements revealed modulation depths of about 4.5% at 2.7 μm, demonstrating favorable saturable absorption characteristics. With the Cr_2Te_3 SAM, we confirmed a stable, passively Q-switched Er:YAP bulk laser. At an absorbed pump power of 6.8 W, pulsed laser output with a pulse energy of 3.7 μJ, a repetition rate of 165.6 kHz, a pulse width of 266 ns, and a peak power of approximately 13.9 W was achieved. These results demonstrate that the Cr_2Te_3 thin film is suitable as a high-speed modulator and holds promise for 2.7 μm mode-locking laser applications.

Author Contributions: Conceptualization, Z.L.; methodology, M.X. and H.M.; formal analysis, S.S.; investigation, H.W., J.C., and Z.L.; resources, T.X.; data curation, H.W.; writing—original draft preparation, H.W.; writing—review and editing, H.W. and T.X.; supervision, T.X. All authors have read and agreed to the published version of the manuscript.

Funding: This research was funded by the National Natural Science Foundation of China (grant number 52502178); the Natural Science Foundation of Henan Province (grant numbers 202300410070 and 252300420975); and the Science and Technology Project in Henan Province (grant numbers 252102310533 and 252102310518).

Data Availability Statement: The original contributions presented in this study are included in the article. Further inquiries can be directed to the corresponding authors.

Conflicts of Interest: The authors declare no conflicts of interest.

References

1. Jiang, M.; Huang, S.; Wang, Z.; Sun, G.; Cai, E.; Lou, F.; Wang, M.; Zhang, S.; Sun, D. A widely tunable mid-infrared Er:YAP laser operating in the 2.7–2.9 μm spectral range. *J. Mater. Chem. C* **2026**, *14*, 15872–15876. [CrossRef]
2. Ren, X.; Wang, Y.; Zhang, J.; Tang, D.; Shen, D. Short-Pulse-Width Repetitively Q-Switched ~2.7 μm Er:Y_2O_3 Ceramic Laser. *Appl. Sci.* **2017**, *7*, 1201. [CrossRef]

3. Xue, Z.; Shen, F.; Li, J.; Liu, X.; Wang, J.; Wang, G.; Liu, K.; Chen, W.; Gao, X.; Tan, T. A MEMS modulator-based dual-channel mid-infrared laser heterodyne radiometer for simultaneous remote sensing of atmospheric CH_4, H_2O and N_2O. *Opt. Express* **2022**, *30*, 31828–31839. [CrossRef] [PubMed]
4. Xue, Z.; Shen, F.; Li, J.; Liu, X.; Wang, G.; Liu, K.; Gao, X.; Chen, W.; Tan, T. MEMS Modulator-Based Mid-Infrared Laser Heterodyne Radiometer for Atmospheric Remote Sensing. *Front. Phys.* **2022**, *10*, 945995. [CrossRef]
5. Xing, T.; Wang, X.; Ou, Z.; Guo, J.; Sun, D.; Chen, H.; Wang, X.; Chen, K.; Gu, Y. Peak-power of 25 W passively Q-switched ~2.8 μm Er:YAP bulk laser based on a reflective $TaSe_2$ saturable absorber mirror. *Opt. Laser Technol.* **2024**, *169*, 110051. [CrossRef]
6. Su, C.; Liang, Y.; Nie, H.; Zhang, B.; Zhang, J.; Liu, J.; Li, T.; Kränkel, C. All-solid-state continuous-wave mode-locked Er:Lu_2O_3 laser at 3 μm. *Opt. Laser Technol.* **2025**, *181*, 111787. [CrossRef]
7. Zhang, Z.; Cheng, Z.; Wang, S.; Guan, C.; Jia, S.; Wang, P. Fabrication of double-cladding fluoroindate glass fibers and watt-level 2.7 μm laser application. *Infrared Phys. Technol.* **2024**, *139*, 105299. [CrossRef]
8. Quan, C.; Sun, D.; Zhang, H.; Luo, J.; Hu, L.; Han, Z.; Dong, K.; Chen, Y.; Cheng, M. 13-W and 1000-Hz of a 2.7-μm laser on the 968 nm LD side-pumped Er:YAP crystal with concave end-faces. *Opt. Express* **2021**, *29*, 21655–21663. [CrossRef] [PubMed]
9. Wang, W.; Xiao, B.; Zhao, P.; Ren, L.; Zhu, S.; Shi, L.; Zhang, X. Nanosecond-Pulsed Passively Q-Switched Fiber Laser by Using Photothermal Dynamics in a Dielectric Microcavity. *ACS Photonics* **2023**, *10*, 3656–3663. [CrossRef]
10. Wang, Z.; Nithyanandan, K.; Coillet, A.; Tchofo-Dinda, P.; Grelu, P. Optical soliton molecular complexes in a passively mode-locked fibre laser. *Nat. Commun.* **2019**, *1*, 830. [CrossRef] [PubMed]
11. He, H.; Hao, Q.; Wang, H.; Yu, S.; Zhou, Y.; Guo, B.; Li, L. 2D Materials-Based Pulsed Solid-State Laser: Status and Prospect. *Laser Photon. Rev.* **2024**, *18*, 1. [CrossRef]
12. Sohail, M.; Shareef, M.; Li, B.; Abdullah, M.; Younis, M.; Wang, M.; Yan, P. Recent advances and challenges of perovskite materials-based saturable absorbers for short-pulsed lasers. *Infrared Phys. Technol.* **2024**, *139*, 105306. [CrossRef]
13. Rafique, M.; Basiri, A.; Bai, J.; Zuo, J.; Yao, Y. Ultrafast Graphene-Plasmonic Hybrid Metasurface Saturable Absorber with Low Saturation Fluence. *ACS Nano* **2023**, *17*, 10431–10441. [CrossRef] [PubMed]
14. Zhang, C.; Chen, Y.; Fan, T.; Ge, Y.; Zhao, C.; Zhang, H.; Wen, S. Sub-hundred nanosecond pulse generation from a black phosphorus Q-switched Er-doped fiber laser. *Opt. Express* **2020**, *28*, 4708–4716. [CrossRef] [PubMed]
15. Xing, T.; Pei, H.; Zhao, M.; Wang, Y.; Jiang, A.; Sun, D.; Chen, H.; Gu, Y. Enhancement of mid-infrared saturable absorption in TiS_2/graphene heterostructure for robust ~2.8 μm passively Q-switched Er:YAP laser. *J. Nonlinear Opt. Phys. Mater.* **2026**, *01*, 2640003. [CrossRef]
16. Du, B.; Pan, H.; Pan, Z.; Chu, H.; Li, Y.; Zhao, S.; Li, D. PdX_2 (X = S, Se) saturable absorbers for passively Q-switched Er:YAP laser at 3 μm. *Opt. Express* **2025**, *33*, 30799–30810. [CrossRef] [PubMed]
17. Xing, X.; Han, Y.; Huang, X.; Chen, W.; Zhang, Z.; Liu, M.; Hu, Q.; Hu, G.; Xian, G.; Zhou, Q.; et al. Small but Efficient: Quasi-1D Topological Insulator β-Bi_4I_4 Nanowires as a Saturable Absorber with High Modulation Depth and Broadband Operation. *Adv. Funct. Mater.* **2026**, *36*, 19204. [CrossRef]
18. Xiao, P.; Sun, X.; Chen, Y.; Han, Y.; Yu, Z.; Liu, W.; Li, X.; Xiao, W.; Yao, Y. Robust Edge States of Quasi-1D Material Ta_2NiSe_7 and Applications in Saturable Absorbers. *Nano Lett.* **2024**, *24*, 10402–10407. [CrossRef] [PubMed]
19. Wu, Q.; Peng, L.X.; Zhao, J.L.; Sun, K.; Chen, S.; Huang, W.C. MXene Nb_2C/MoS_2 heterostructure: Nonlinear optical properties and a new broadband saturable absorber for ultrafast photonics. *Mater. Today Phys.* **2025**, *52*, 101678. [CrossRef]
20. Xing, T.; Wang, X.; Pei, H.; Jiang, A.; Sun, D.; Zhang, J.; Gu, Y. Short-pulsed passively Q-switched ~2.8 μm bulk laser based on VS_2/tellurene composite saturable absorber. *Opt. Commun.* **2025**, *596*, 132452. [CrossRef]
21. Zhang, S.; Hu, X.; Kong, X.; Zhao, J.; Sun, G.; Wang, H.; Cai, E.; Zhang, Q.; Li, S.; Wang, X.; et al. Enhanced 2.7 μm wavelength sub-80 ns pulse generation via iron-chromium co-doped ZnS polycrystalline. *Opt. Express* **2025**, *33*, 15141–15148. [CrossRef] [PubMed]
22. Li, B.; Pan, H.; Pan, Z.; Chu, H.; Li, Y.; Zhao, S.; Li, D. Two-dimensional violet phosphorus as a broadband saturable absorber for mid-infrared photonics. *Opt. Express* **2025**, *33*, 21328–21338. [CrossRef] [PubMed]
23. Tiwari, N.; Gowda, C.; Mishra, S.; Pandey, P.; Talapatra, S.; Chaudhary, V.; Singh, A.; Tiwary, C. Magnetocaloric effect observations near room temperature in few-layered chromium telluride (Cr_2Te_3). *Nanoscale* **2026**, *18*, 1994–2007. [CrossRef] [PubMed]
24. Purwar, S.; Bhowmik, T.K.; Ghorai, S.; Thirupathaiah, S. 3D-Ising-type magnetic interactions stabilized by the extremely large uniaxial magnetocrystalline anisotropy in layered ferromagnetic Cr_2Te_3. *Mater. Today Phys.* **2024**, *46*, 101522. [CrossRef]
25. Luo, F.; Zhang, J.; Wang, Z.; Tang, F.; Fang, Y.; Zhou, W. The effect of Mn doping on the electrical and magnetic properties of Cr_2Te_3 thin films. *J. Magn. Magn. Mater.* **2024**, *610*, 172591. [CrossRef]
26. Chen, B.; Lan, J.; Tsai, M.; Lee, K.; Khim, Y.; Lee, I.; Chang, Y.; Lee, J.; Lee, C. Optical nonlinear refractive index measurements of Cr_2Te_3 with an immense photothermal effect. *Mater. Adv.* **2025**, *6*, 1345–1352. [CrossRef]
27. Lee, K.; Lee, I.; Khim, Y.; Kwon, S.; Lim, G.; Jung, J.; Chang, Y.; Lee, J. Nonlinear optical properties of PVD-grown Cr_2Te_3 film and its nonlinear switching application. *J. Alloys Compd.* **2023**, *956*, 170308. [CrossRef]

28. Zhong, Y.; Peng, C.; Huang, H.; Guan, D.; Hwang, J.; Hsu, K.; Hu, Y.; Jia, C.; Moritz, B.; Lu, D.; et al. From Stoner to local moment magnetism in atomically thin Cr_2Te_3. *Nat. Commun.* **2023**, *14*, 5340. [CrossRef] [PubMed]
29. Ranabhat, R.; Almutairi, S.; Yu, M. Half-metallicity induced by Cr atoms on the surface of ultra-thin Cr_2Te_3 film: First principles study. *Nanotechnology* **2026**, *37*, 045706. [CrossRef] [PubMed]
30. Mondal, R.; Mathias, R.; Bastos, L.; Gowda, C.; Tiwari, N.; Singh, H.; Woellner, C.; Tiwary, C.; Kumbhakar, P. Two-dimensional chromium telluride-coated 3D-printed architectures for energy harvesting. *Nanoscale* **2025**, *17*, 14647–14659. [CrossRef] [PubMed]
31. Ou, Z.; Wang, X.; Zhu, B.; Sun, D.; Xing, T.; Gu, Y. Enhancement of mid-infrared saturable absorption of graphene by compositing with PbSe for ultra-short pulse lasers in the ~2.8 to ~4 μm band. *Infrared Phys. Technol.* **2024**, *136*, 105056. [CrossRef]
32. Zhang, H.; Liu, Y.; Feng, T.; Zhao, S.; Qiao, W. Optical modulation properties of the Ni-based layered double hydroxides for dual-wavelength Q-switched Er:YAP laser at 2.7 μm. *Opt. Mater.* **2023**, *137*, 113499. [CrossRef]
33. Li, S.; Yuan, J.; Liu, Q.; Wang, Z.; Xing, F.; Zhang, F. Passively Q-switched near-infrared and visible lasers employing two-dimensional violet phosphorus nanosheets as saturable absorbers. *Infrared Phys. Technol.* **2026**, *156*, 106569. [CrossRef]
34. Li, C.; Zang, Z.; Han, C.; Hu, Z.; Tang, X.; Du, J.; Leng, Y.; Sun, K. Highly compact $CsPbBr_3$ perovskite thin films decorated by ZnO nanoparticles for enhanced random lasing. *Nano Energy* **2017**, *40*, 195. [CrossRef]
35. Lv, M.; Zhao, J.; Guo, L.; Zhang, Y.; Zhao, Q.; Teng, L.; Wang, M.; Zhang, S.; Wang, X. Nonlinear optical response of Au/CsPbI3 quantum dots and its laser modulation characteristics at 2.7 μm. *Micromachines* **2024**, *15*, 1043. [CrossRef] [PubMed]
36. Kong, X.; Hu, X.; Qi, C.; Du, L.; Wang, M.; Liu, Q.; Zhang, S. Two-dimensional tin diselenide as the saturable absorber for passively Q-switched Er:YAP 3 μm solid-state laser. *Laser Phys.* **2023**, *33*, 125802. [CrossRef]

Disclaimer/Publisher's Note: The statements, opinions and data contained in all publications are solely those of the individual author(s) and contributor(s) and not of MDPI and/or the editor(s). MDPI and/or the editor(s) disclaim responsibility for any injury to people or property resulting from any ideas, methods, instructions or products referred to in the content.